Taylor & Francis
Taylor & Francis Group

LABORATORY STUDY

🔓 OPEN ACCESS | Check for updates

Integration of mitochondrial gene expression and immune landscape in acute kidney injury prediction

Xiaoping Xia[a], Renyang Liu[b] and Xiaohui Jiang[b] 🆔

[a]Department of Intensive Care Unit, Taizhou Integrated Traditional Chinese and Western Medicine Hospital, Wenling, Zhejiang, China; [b]Emergency and Critical Care Center, Intensive Care Unit, Zhejiang Provincial People's Hospital, Affiliated People's Hospital, Hangzhou Medical College, Hangzhou, Zhejiang, China

ABSTRACT

Background: Acute kidney injury (AKI) is a life-threatening condition with limited early biomarkers. Mitochondrial dysfunction is central to AKI pathophysiology, yet its potential for predicting AKI remains underexplored.

Methods: Gene expression data from three publicly available AKI datasets (GSE30718, GSE61739, and GSE139061) were analyzed to identify differentially expressed genes (DEGs). A set of 11 mitochondrial-related genes was selected and used to construct a mitochondrial risk score (MRS) model *via* Lasso and elastic net regression. The model was validated across multiple datasets. Immune infiltration was assessed using the xCell algorithm to explore the relationship between MRS and immune cell dynamics in AKI. Stable HK-2 cells were constructed of XRCC3 knockdown and overexpression to investigate the effects of XRCC3 on cell activities. Additionally, the impact of XRCC3 on mitochondrial structure and function was examined *in vivo* and *in vitro*.

Results: Eleven mitochondrial-related genes were consistently dysregulated across all datasets. PCA demonstrated a clear separation between AKI and normal samples. Functional enrichment analysis revealed that upregulated genes were linked to extracellular matrix remodeling and stress responses, while downregulated genes were associated with mitochondrial dysfunction. The MRS model showed strong predictive performance. We found that XRCC3 significantly promoted the activities of HK-2 cells and improved the integrity of mitochondrial structure and function *in vivo* and *in vitro*.

Conclusion: The mitochondrial gene-based MRS model is a robust tool for predicting AKI. Our findings underscore the critical role of mitochondrial dysfunction and immune modulation in AKI, offering potential avenues for targeted therapeutic strategies.

1. Introduction

Acute Kidney Injury (AKI) is a critical and rapidly progressing condition characterized by an abrupt decline in renal function, which significantly contributes to global morbidity and mortality [1]. It is particularly prevalent in patients with underlying comorbidities or those in intensive care settings, where it often complicates the course of critical illness [2]. AKI manifests as a sudden reduction in glomerular filtration rate (GFR), leading to the retention of metabolic waste products, fluid imbalance, and electrolyte disturbances [3]. The etiology of AKI is multifactorial, encompassing ischemia, nephrotoxic agents, infections, and systemic inflammation [4]. Despite advances in critical care, the diagnosis and

treatment of AKI remain challenging, with no reliable biomarkers for early detection, leading to delays in appropriate intervention and poor patient prognosis. Early diagnosis of AKI is essential to mitigate its long-term consequences, including progression to chronic kidney disease (CKD) [5].

Mitochondrial dysfunction has been increasingly recognized as a central factor in the pathophysiology of AKI. Mitochondria are critical to cellular energy production, calcium regulation, and the modulation of oxidative stress, apoptosis, and inflammation [6]. In AKI, mitochondrial damage is commonly associated with disruptions in mitochondrial dynamics, including the processes of fission and fusion, which are crucial for maintaining mitochondrial integrity and function. The role of mitochondrial

dysfunction in AKI is further compounded by its involvement in regulating apoptosis and inflammation, two key processes that drive the progression of kidney injury [7,8]. Furthermore, mitochondrial dysfunction is not only a consequence of AKI but also a potential driver of CKD progression following an acute insult [9]. The transition from AKI to CKD is marked by persistent mitochondrial damage and impaired repair mechanisms, which can contribute to long-term renal dysfunction [10]. This underscores the importance of therapeutic strategies targeting mitochondrial health to prevent the progression of kidney disease [11]. Given the pivotal role of mitochondria in AKI, targeting mitochondrial dysfunction holds therapeutic potential; however, the precise molecular pathways remain incompletely understood. Identifying mitochondrial-related biomarkers could improve early detection and provide new avenues for therapeutic intervention.

In our study focused on biomarker discovery and the construction of a prognostic model for AKI using bioinformatics, we noted that research by Wang et al. identified SLC2A1 as a key regulator of ferroptosis that plays a significant role in the progression of AKI [12]. Li et al. identified three core apoptosis-related genes: BFB, EGF, and COL1A1, as biomarkers for AKI, which were found to be associated with immune infiltration in AKI [13]. Furthermore, Yang et al. explored AKI biomarkers from the perspective of sepsis [14]. In contrast, our research specifically focuses on mitochondria-related genes, identifying potential biomarkers for AKI from the mitochondrial perspective, an approach that has not been previously reported in the literature.

In this study, we aim to develop a mitochondrial gene-based predictive model for AKI by analyzing gene expression data from three publicly available datasets. We will identify mitochondrial-related genes consistently dysregulated across multiple datasets, thereby constructing a robust predictive model for early AKI detection. Additionally, we will explore the relationship between mitochondrial dysfunction and immune cell infiltration in AKI, shedding light on the interplay between metabolic disturbances and immune responses. The findings from this study could significantly enhance our understanding of AKI pathophysiology and provide potential biomarkers for early diagnosis, ultimately guiding more effective clinical management and therapeutic interventions.

2. Methods

2.1. Differential gene expression analysis and data integration

In this study, we utilized three publicly available AKI datasets, GSE30718, GSE61739, and GSE139061, which compromised with 47 samples, 96 samples, and 48 samples from homo sapiens respectively, sourced from the Gene Expression Omnibus (GEO) for comprehensive bioinformatics analysis. These datasets include gene expression profiles from both AKI and healthy control samples. And mitochondria-related genes were extracted from the study conducted by Zhang

et al. [15]. After preprocessing and normalization of the raw data, differential expression analysis was conducted using the limma package in R. Given that the number of mitochondria-related genes is only 2030, while the number of differentially expressed genes associated with AKI is severalfold higher than that of mitochondria-related genes. To further explore the relationship between these two groups, we set the threshold of |logFC| for differentially expressed genes at 0.5, which allows for the inclusion of more genes and increases the overlap rate. To investigate the role of mitochondrial dysfunction in AKI, mitochondrial-related genes were selected based on annotations from the Kyoto Encyclopedia of Genes and Genomes (KEGG) and Gene Ontology (GO) databases. The DEGs from each dataset were then cross-referenced with this mitochondrial gene list, leading to the identification of 11 genes that were consistently dysregulated across all three datasets. These 11 genes were subjected to principal component analysis (PCA), which effectively separated AKI from normal samples based on gene expression, further supporting their potential as biomarkers for AKI.

2.2. Functional enrichment analysis of differentially expressed genes in AKI

To explore the molecular alterations in AKI, all upregulated or downregulated genes were then subjected to functional enrichment analysis, including GO analysis to explore biological processes (BPs), cellular components (CCs), molecular functions (MFs), and KEGG pathway analysis to investigate the underlying biological pathways through 'clusterProfiler' package in R, with an adjusted p-value <0.05 set as the threshold for statistical significance.

2.3. Construction of a mitochondrial gene-based predictive model for AKI

To develop a robust predictive model for AKI, a set of 11 mitochondrial-related genes was selected. The GSE30718 dataset was used as the training cohort, while GSE139061 and GSE61739 served as independent validation cohorts. Lasso regression with 10-fold cross-validation was applied to identify the most informative genes for AKI prediction. The selected genes were further examined for pairwise correlations, and elastic net regression was employed to construct a predictive model. Based on the weights of the nine selected genes, the mitochondrial risk score (MRS) for each patient was calculated. The model's performance was evaluated by assessing the prediction probabilities of AKI samples in the training set.

2.4. Model validation of MRS in AKI

To validate the predictive performance of the MRS model, differential expression analysis was performed across the three datasets (GSE30718, GSE139061, and GSE61739). The MRS of AKI and normal samples were compared, followed by

ROC curve analysis for both the nine model genes and MRS. The model's performance was assessed by calculating the area under the curve (AUC) for both individual genes and MRS.

2.5. Integration of PPI and disease mechanism analysis

To explore the biological relevance of the nine selected genes, a protein-protein interaction (PPI) network was constructed using data from the STRING database [16]. Additionally, the Comparative Toxicogenomics Database (CTD) [17] was utilized to integrate chemical-gene/protein interactions, chemical-disease associations, and gene-disease relationships, facilitating the identification of key genes involved in AKI and providing insights into their potential roles in disease pathogenesis.

2.6. Immune infiltration analysis and its association with MRS in AKI

To investigate the relationship between the MRS and immune cell infiltration in AKI, immune-related features were analyzed using the xCell algorithm [18]. Differential expression of immune cell signatures between AKI and normal samples was assessed, and immune landscape differences were explored between patients with high and low MRS. Furthermore, the correlation between the nine selected model genes and ImmuneScore was evaluated to elucidate the role of these genes in immune modulation within the AKI context.

2.7. Cell culture

The human renal proximal tubular epithelial cell of HK-2 was obtained from the American Type Culture Collection (ATCC). The cell was cultured in 90% Dulbecco's Modified Eagle Medium (DMEM) supplemented with 10% fetal bovine serum (FBS) and 1% penicillin/streptomycin. The cultures were maintained in a humidified incubator at 37°C with 5% CO_2.

2.8. Construction of stable cell lines

A lentiviral-based shRNA approach was employed to utilize three distinct shRNA sequences. The shRNA sequences were cloned into a lentiviral vector (pLKO.1) to knock down the expression of XRCC3, while a full-length XRCC3 cDNA was synthesized and subsequently cloned into a lentiviral overexpression vector (pLVX) to achieve XRCC3 overexpression in HK-2 cell. In addition, nontargeting shRNA served as the negative control. 293T cells were then utilized to package the lentivirus. HK-2 cells were seeded in 6-well plates at 60–70% confluence, after which lentiviral particle constructs were added to the cells in the presence of polybrene (8 μg/mL) to enhance viral transduction. The cells were incubated with the virus for 12–16 h, after which the medium was replaced with a fresh culture medium. Following 48 h of infection,

puromycin was used to screen for successful transduction. The effects of XRCC3 knockdown and overexpression were confirmed through quantitative reverse transcription polymerase chain reaction (qRT-PCR) analyses. The resulting stable cell lines were then employed for downstream functional assays. The sequences for XRCC3 knockdown and overexpression are shown in Table S1.

2.9. RNA extraction and qRT-PCR

Total RNA was extracted from cells and tissues using the TRIzol reagent. Subsequently, 1 μg of RNA was subjected to reverse transcription, during which genomic DNA was removed, and amplification was performed according to the instructions provided in the reverse transcription kit, resulting in the conversion of RNA to cDNA. Following this, cDNA amplification was carried out using Fast Start Universal SYBR Green Master through real-time PCR. The relative quantification of the target gene was conducted using the 2-ΔΔCt method, with GAPDH serving as an internal control. The primer sequences used are listed in Table S2.

2.10. CCK8 assay

The capacity for cell proliferation was assessed using CCK8 kits. Transfected cells were seeded in 96-well plates at a density of 1,000 cells per well. Following cell adherence, the CCK8 solution was added, and the cells were cultured for an additional 2 h. At this point, the absorbance of each well was measured at 450 nm, establishing the initial value. Subsequently, absorbance measurements were conducted daily for 3 days, maintaining the same time of measurement each day.

2.11. EdU assay

HK-2 cells were cultured in 24-well plates and incubated overnight. The cells were subsequently treated with 10 μM EdU for 2 h. Following incubation, the cells were fixed with 4% paraformaldehyde for 15 min and then permeabilized using 0.5% Triton X-100 for 20 min. EdU incorporation was assessed using the EdU Assay Kit (Elabscience, China) following the manufacturer's instructions. The cells were subsequently stained with DAPI to visualize the nuclei, and the percentage of EdU-positive cells was determined using fluorescence microscopy.

2.12. Transwell assay

A total of 2×10^5 HK-2 cells were resuspended in 500 μL of serum-free DMEM and seeded into the upper chamber, while the lower chamber was supplemented with DMEM containing 10% FBS. After a specified incubation period, non-migratory cells in the upper chamber were thoroughly removed. The cells that migrated to the lower chamber were fixed with methanol and subsequently stained with 0.1% crystal violet dye for

15 min. Finally, the neutral resin was applied for sealing, and the number of cells in six randomly selected fields at a magnification of 20X was counted using an inverted microscope.

2.13. Apoptosis assay of Annexin V/PI

An Annexin V/PI staining assay was conducted to access cell apoptosis. HK-2 cells were cultured in 6-well plates and subjected to the designated experimental conditions. Following treatment, these cells were acquired *via* trypsinization, washed twice with cold PBS, and resuspended in the binding buffer. A total of 1×10^6 cells were then incubated with 5 μL of Annexin V-FITC and 5 μL of PI solution for 15 min at room temperature in the dark. After the incubation, 400 μL of binding buffer was added to each sample, and these cells were analyzed immediately using flow cytometry (BD FACSCanto).

2.14. Mitochondrial membrane potential JC-1

HK-2 cells were cultured in 6-well plates at a density of 1×10^5 to 2×10^5 cells per well and allowed to adhere and proliferate for 24 h in a 37 °C incubator with 5% CO_2. Following this incubation, the cells were treated under specific experimental conditions and gently washed with PBS. Then detached cells using trypsin/EDTA for 5 to 10 min at 37 °C. The resulting cell suspension was collected and centrifuged at 300–400 g for 5 min. After discarding the supernatant, the cell pellet was resuspended in 1 mL of fresh culture medium or PBS. An aliquot of 0.5 to 1×10^6 cells was transferred to a new tube, and JC-1 dye was added to the cell suspension according to the manufacturer's instructions. The cells were incubated in the dark at 37 °C for 20 to 30 min. The cells were analyzed immediately using flow cytometry, with settings adjusted to detect the red fluorescence of J-aggregates (indicative of a high mitochondrial membrane potential) and the green fluorescence of JC-1 monomers (indicative of a low mitochondrial membrane potential). Appropriate fluorescence detection channels were used, specifically 585 nm for red fluorescence and 530 nm for green fluorescence.

2.15. Mitochondrial structure detecting

Electron microscopy was utilized to examine structural alterations in the mitochondria, while immunofluorescence staining was employed to observe changes in mitochondrial fluorescence.

Samples were fixed in 2.5% glutaraldehyde (prepared in phosphate-buffered saline) for 2 h, followed by rinsing with 0.1 M phosphate buffer. The samples were then fixed in 1% osmium tetroxide solution for 2 h and rinsed again with 0.1 M phosphate buffer. Subsequently, dehydration was performed using a graded series of ethanol at 4 °C. The samples were treated at room temperature for 4 h with a mixture of pure acetone and embedding medium (2:1), followed by overnight treatment with a mixture of pure acetone and embedding medium (1:2). They were then incubated at 37 °C for 3 h in pure embedding medium. Ultrathin sections, approximately 50 nm in thickness, were obtained using an ultramicrotome. The sections were double-stained with 3% uranyl acetate and lead citrate and examined using a transmission electron microscope for imaging.

HK-2 cells were seeded in 24-well plates, wherein the cells were cultured to an appropriate density before discarding the culture medium. A working solution of MitoTracker was prepared by diluting the dye in PBS or culture medium to ensure an appropriate concentration. The MitoTracker working solution was pre-warmed to 37 °C, then added to the cells, and they were incubated at 37 °C for 15–45 min. After incubation, the staining solution was discarded, and the cells were washed with PBS. The fresh culture medium was added for continued culture or observation. After staining, cells were washed again with PBS. Cells were fixed with 4% paraformaldehyde for 10–15 min. The fixation solution was discarded, and the cells were washed with PBS once more. Cells were permeabilized with 0.3% Triton X-100 for 10 min. Finally, observations were made using a fluorescence microscope.

2.16. IRI induced AKI model

Ischemia-reperfusion injury (IRI) induced AKI models were constructed *via* 8-week-old healthy male C57BL/6J mice. Mice were anesthetized to maintain a stable state throughout the surgical procedure. Following the shaving of their abdominal fur, the surgical site was disinfected using alcohol or povidone-iodine. An incision was made along the abdominal midline to expose the abdominal musculature and peritoneum, which was then carefully opened to reveal the internal organs. The intestines were gently retracted to access the kidneys, allowing for exposure of the renal pedicle. A microvascular clamp was applied to the right renal pedicle for 30 min, and the duration of ischemia was recorded as the kidney transitioned in color from red to deep purple, indicating successful occlusion. After noting this color change, the kidney was repositioned in the abdominal cavity, and the left renal pedicle was subsequently clamped for 30 min, with its ischemic duration also recorded. The interval between clamping the left and right renal pedicles was approximately 1–1.5 min. Once a sufficient ischemic period had elapsed, the arterial clamp was released to initiate reperfusion, during which the kidney regained its red color, and the reperfusion duration was about 45 min. The muscle layer and skin were sutured, and each mouse received an intraperitoneal injection of 0.5 mL of warm sterile saline. Finally, the mice were placed on a heating pad until fully recovered from anesthesia. The morphological changes in renal tissue were assessed through H&E staining to determine the success of the model establishment. Subsequently, mitochondrial immunofluorescence staining was performed on both normal renal tissue and injured renal tissue to evaluate mitochondrial integrity. Additionally, electron microscopy was employed to examine the structural characteristics of the mitochondria.

2.17. LPS induced AKI model

A total of 18 eight-week-old healthy male C57BL/6J mice were randomly assigned to two groups: control and lipopolysaccharide (LPS), with 9 mice in each group. AKI was induced by administering an intraperitoneal injection of LPS at a dose of 10 mg/kg, while a saline solution served as the control. After a 24-h period post-injection, the mice were euthanized, and blood and kidney tissues were collected for analysis. Specifically, we euthanized mice using a high-dose tail vein injection of pentobarbital sodium (150 mg/kg). Throughout the process, the mice were in an anesthetized (unconscious) state. After referring to the AVMA Animal Euthanasia Guidelines (2020), the mice were euthanized due to cervical dislocation. The animal experiments we conducted were approved by the Institutional Animal Care and Use Committee of the Hubei Provincial Center for Disease Control and Prevention (license number: 202410107). The extent of renal injury was assessed through hematoxylin and eosin (HE) staining, and the mitochondrial integrity and structure were evaluated through mitochondrial immunofluorescence staining and electron microscopy.

2.18. HE staining

HE staining was employed to evaluate the histological features of renal tissues in AKI mouse models. Normal renal tissue and injured renal tissue were fixed in 10% formalin, embedded in paraffin blocks, and sectioned into 5-micron thick slices placed on microscope slides. Following deparaffinization and rehydration, the sections were stained with hematoxylin to visualize the cell nuclei and subsequently counterstained with eosin to accentuate the cytoplasm. The stained sections were then examined under a microscope, and images were captured for further analysis.

2.19. Immunofluorescence assay

The tissues were collected and fixed with 4% formaldehyde for 15 min, followed by three washes with PBS. The cells were then permeabilized at room temperature using 0.5% Triton X-100 for 20 min. Next, an antibody specific to XRCC2 was added for staining, followed by DAPI staining to visualize the nuclei in the dark for 30 min, then secondary antibodies with fluorescent labels the next day. Finally, fluorescence was observed using a fluorescent microscope.

3. Results

3.1. Identification of differentially expressed mitochondrial genes and PCA

Differential expression analysis across the three datasets (GSE30718, GSE61739, and GSE139061) revealed consistent dysregulation of several mitochondrial-related genes, as illustrated in the volcano plots (Figure 1(a)). Due to the limited number of intersecting genes, all genes with |logFC| > 0.5 were retained for subsequent analysis, ensuring a comprehensive exploration of potential biomarkers. The intersection of the DEGs with mitochondrial genes identified a core set of 11 genes, which were significantly altered across all three datasets (Figure 1(b)). To assess the discriminative power of these 11 genes, PCA was performed, and the results demonstrated a distinct separation between AKI and normal samples based on the expression patterns of these genes, highlighting their potential as robust biomarkers for AKI detection (Figure 1(c)).

3.2. Functional enrichment analysis of upregulated and downregulated genes in AKI
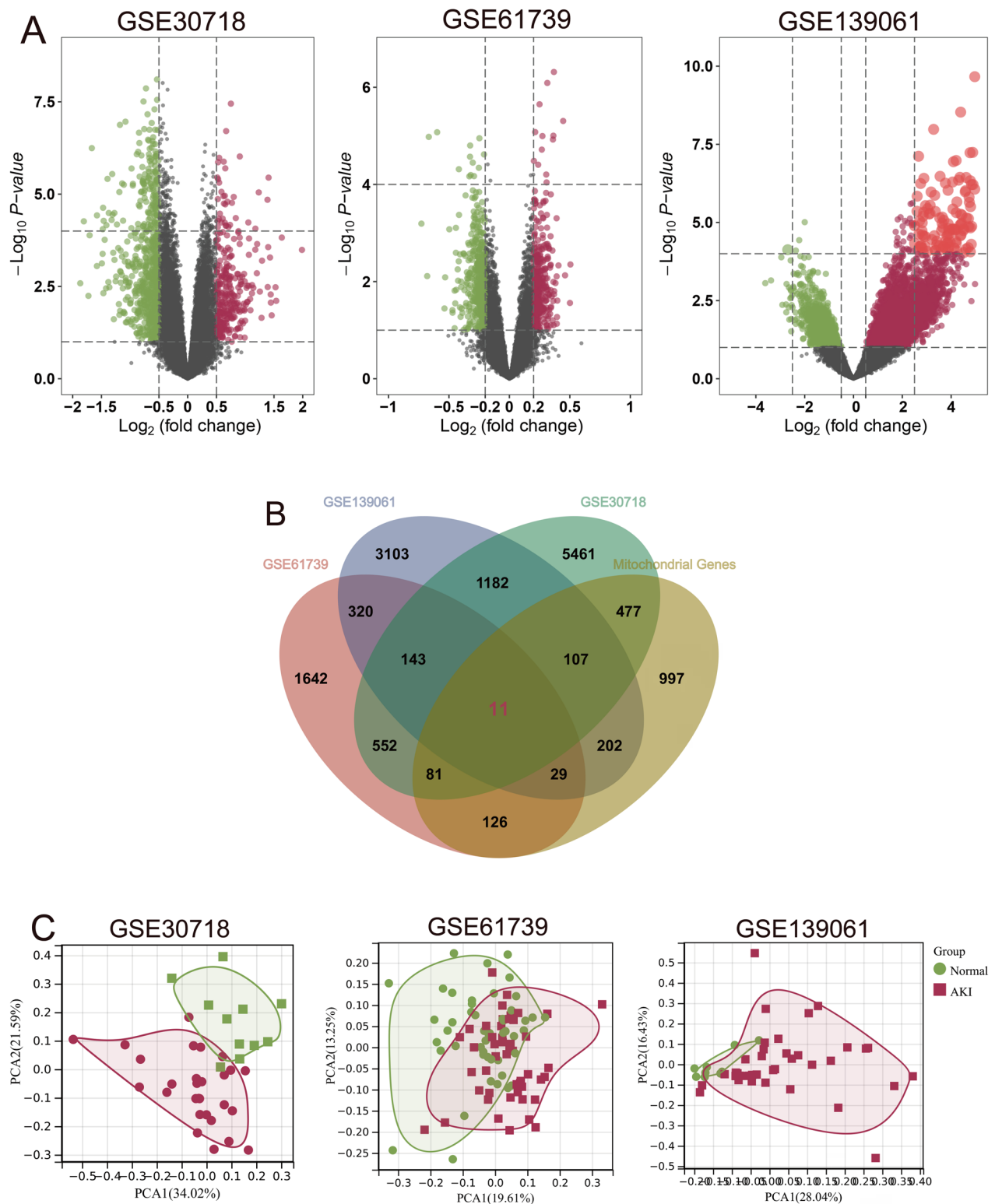
The differential gene expression analysis identified 1,079 upregulated genes (Figure 2(a)) and 1,745 downregulated genes (Figure 2(b)). GO enrichment analysis revealed that upregulated genes were enriched in processes related to the collagen-containing extracellular matrix, endoplasmic reticulum lumen, and regulation of neurotransmitter levels, suggesting their involvement in extracellular matrix remodeling and cellular stress responses in AKI (Figure 2(c)). Conversely, downregulated genes were predominantly associated with mitochondrial functions, including the mitochondrial matrix, mitochondrial inner membrane, and cellular amino acid metabolism, indicating potential mitochondrial dysfunction in AKI (Figure 2(d)). KEGG pathway analysis identified significant enrichment in pathways for upregulated genes, such as Salmonella infection, Neuroactive ligand-receptor interaction, and Human T-cell leukemia virus 1 infection (Figure 2(e)). Downregulated genes were primarily enriched in pathways like Tryptophan metabolism, Carbon metabolism, and Nonalcoholic fatty liver disease (Figure 2(f)), highlighting key metabolic disturbances in AKI.

3.3. Mitochondrial gene-based model performance and risk score calculation in AKI

Lasso regression analysis (Figure 3(a-b)) revealed 9 out of the 11 mitochondrial-related genes as significant contributors to the model, with 10-fold cross-validation confirming the stability and reliability of these genes. Correlation analysis (Figure 3(c)) demonstrated the interrelationships between the nine selected genes across both the training and validation datasets. Elastic net regression (Figure 3(d)) showed that all nine genes were retained in the final model, with XRCC3 contributing the most to AKI prediction, while PGR had the least influence. Based on the weights of these genes, the MRS was calculated for each patient, providing a quantitative measure of AKI risk. The model's predictive performance was assessed in the training cohort (Figure 3(e)), where AKI samples exhibited high prediction probabilities (close to 1), while normal samples were assigned significantly lower probabilities, confirming the model's robust discriminatory power.

3.4. Performance of the MRS model in AKI

Differential expression analysis (Figure 4(a)) revealed that the MRS was significantly higher in AKI samples compared to

Figure 1. Differential gene expression and PCA analysis of AKI-associated mitochondrial genes.
(a) Volcano plots illustrating the differential expression of genes across the GSE30718, GSE61739, and GSE139061 datasets, comparing AKI samples to normal controls. (b) Venn diagram depicting the intersection of differentially expressed genes and mitochondrial-related genes, highlighting 11 common genes identified across the datasets. (c) PCA based on the 11 intersecting genes, showing a distinct clustering of AKI samples separate from normal controls.

normal samples across all three datasets, supporting the relevance of MRS in distinguishing AKI from healthy controls. ROC curve analysis (Figure 4(b)) of the nine selected genes

demonstrated variable predictive performance. However, MRS (Figure 4(c)) showed superior predictive accuracy, with AUC values of 1.0 in GSE30718, 0.91 in GSE139061, and 0.75 in
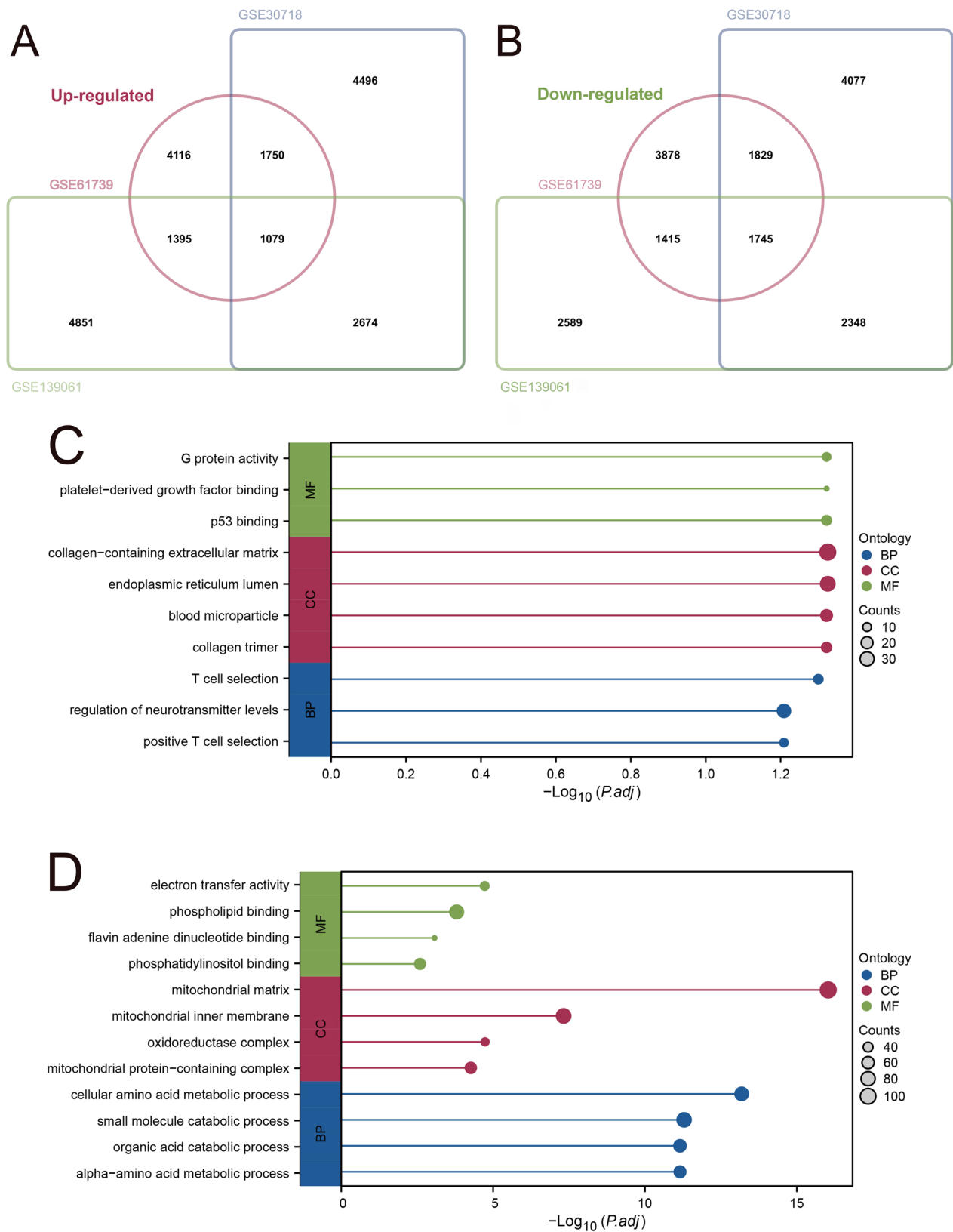
Figure 2. Enrichment analysis of differentially expressed genes in AKI.
(A-B) Venn diagrams showing the upregulated (A) and downregulated (B) genes identified across the three datasets. (C-D) GO enrichment analysis of upregulated (C) and downregulated (D) genes, highlighting key BPs, CCs, and MFs. (E-F) KEGG pathway analysis of upregulated (E) and downregulated (F) genes, revealing significant pathway enrichment related to inflammation, cellular stress, and metabolic processes.
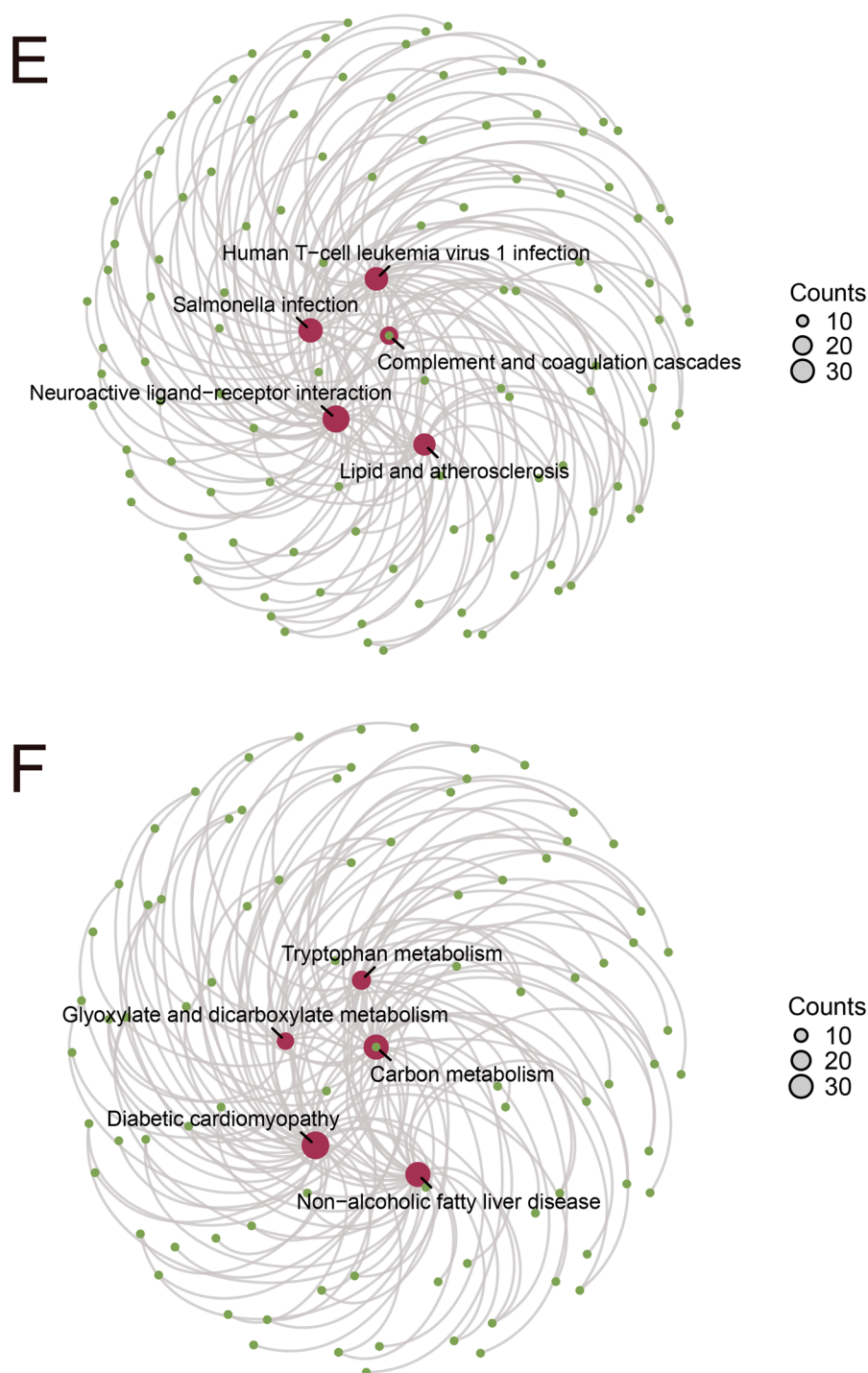
E

Human T−cell leukemia virus 1 infection

Salmonella infection

Complement and coagulation cascades

Neuroactive ligand−receptor interaction

Lipid and atherosclerosis

Counts
○ 10
○ 20
○ 30

F

Tryptophan metabolism

Glyoxylate and dicarboxylate metabolism

Carbon metabolism

Diabetic cardiomyopathy

Non−alcoholic fatty liver disease

Counts
○ 10
○ 20
○ 30

Figure 2. (Continued)

GSE61739, indicating robust performance in distinguishing AKI from normal samples.

3.5. Results of PPI and disease Mechanism analysis

The PPI network (Figure 5(a)), constructed based on the STRING database, highlighted the interactions among the nine selected genes, offering insights into their functional connectivity and underlying cellular processes. Analysis using the CTD database (Figure 5(b)) revealed that all nine genes were implicated in AKI-related gene networks, underscoring their relevance in the pathophysiology of AKI. Furthermore, the inference scores for these genes (Figure 5(c)) in the context of AKI indicated that HMGCS2 exhibited the highest score, suggesting its critical involvement in AKI, while XRCC3 also showed a notable score, indicating its potential contribution to AKI risk.
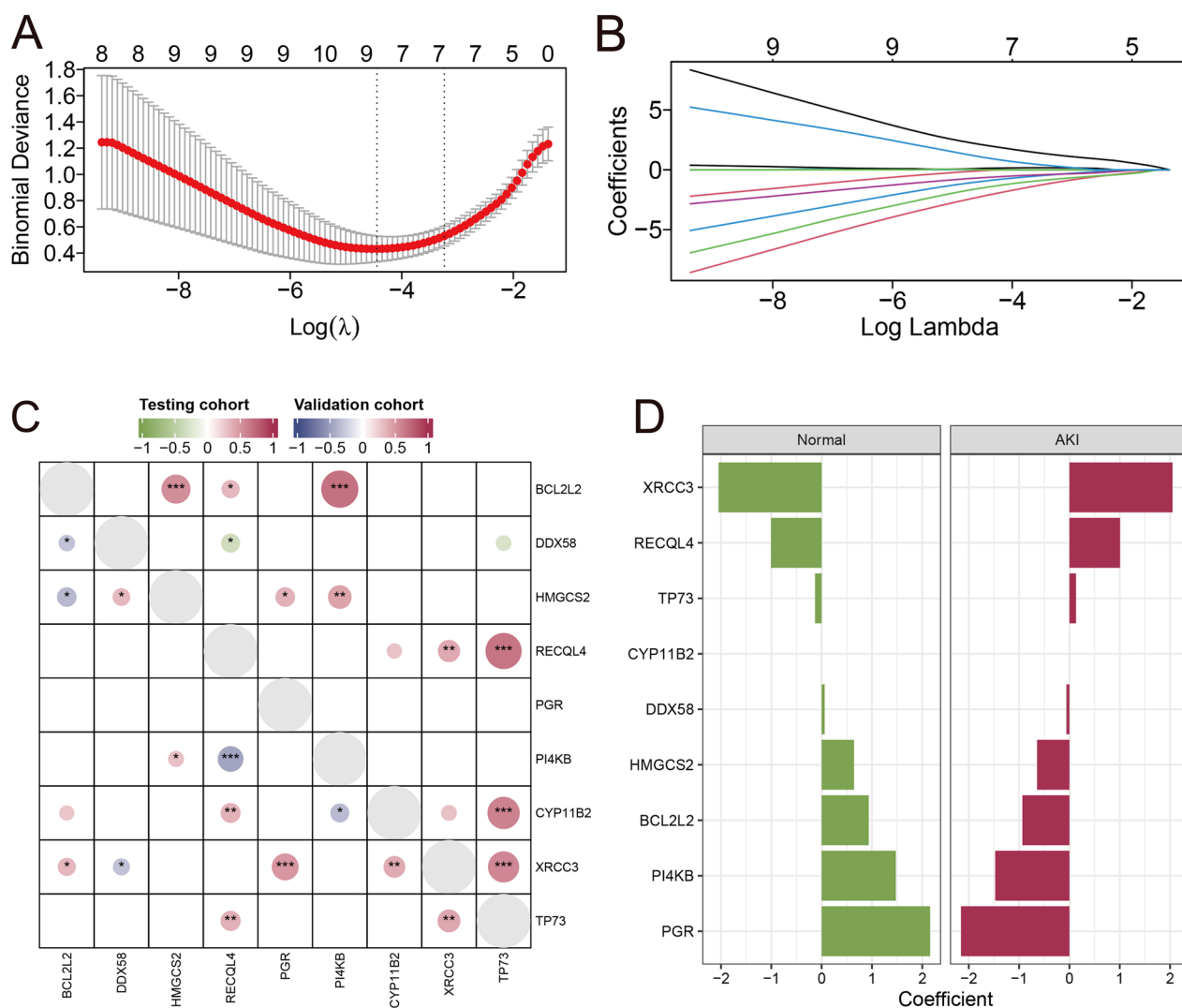
Figure 3. Development of a mitochondrial gene-based predictive model for AKI.
(A-B) Lasso regression analysis identifying nine key genes selected for the model after 10-fold cross-validation. (C) Correlation analysis of the nine selected genes in both the training and validation datasets. (D) Elastic net regression modeling of the nine selected genes, highlighting the individual contributions of each gene to AKI prediction, with XRCC3 showing the greatest influence. (E) Performance evaluation of the model in the training set, with AKI samples showing high prediction probabilities (close to 1), indicating strong model discrimination between AKI and normal samples.

3.6. Immune landscape and MRS correlation in AKI

Immune infiltration analysis using the xCell algorithm revealed significant differences in the expression of immune-related features between AKI and normal samples, suggesting substantial alterations in the immune response during AKI (Figure 6(a)). In comparing immune scores, patients with higher MRS exhibited significantly elevated ImmuneScores compared to those with lower MRS, indicating that higher mitochondrial risk correlates with enhanced immune activation in AKI (Figure 6(b)). Furthermore, correlation analysis showed a strong association between the nine selected model genes and ImmuneScore, suggesting that these genes contribute to immune cell infiltration and immune modulation in AKI (Figure 6(c)). Based on the combination of inference score and PPI analysis, we found that XRCC3 and BCL2L2 exhibited significant protein interaction capabilities and were ranked among the top five genes.

Additionally, immunoinfiltration analyses indicated that the MRS-high group demonstrated more severe immune infiltration, with XRCC3 showing a positive correlation with Immunescore, while BCL2L2 displayed a negative correlation. Additionally, elastic net regression showed that all nine genes were retained in the final model, with XRCC3 contributing the most to AKI prediction. Consequently, we selected XRCC3 as the focus of our subsequent experimental validation.

3.7. The effect of XRCC3 on HK-2 cell functions

To investigate the role of XRCC3 in AKI, we conducted a series of functional experiments. First, we successfully established XRCC3 knockdown and overexpression models in HK-2 cells using lentiviral interference (Figure 7(a-b)). The results of CCK8 and EdU assays indicated that XRCC3 significantly
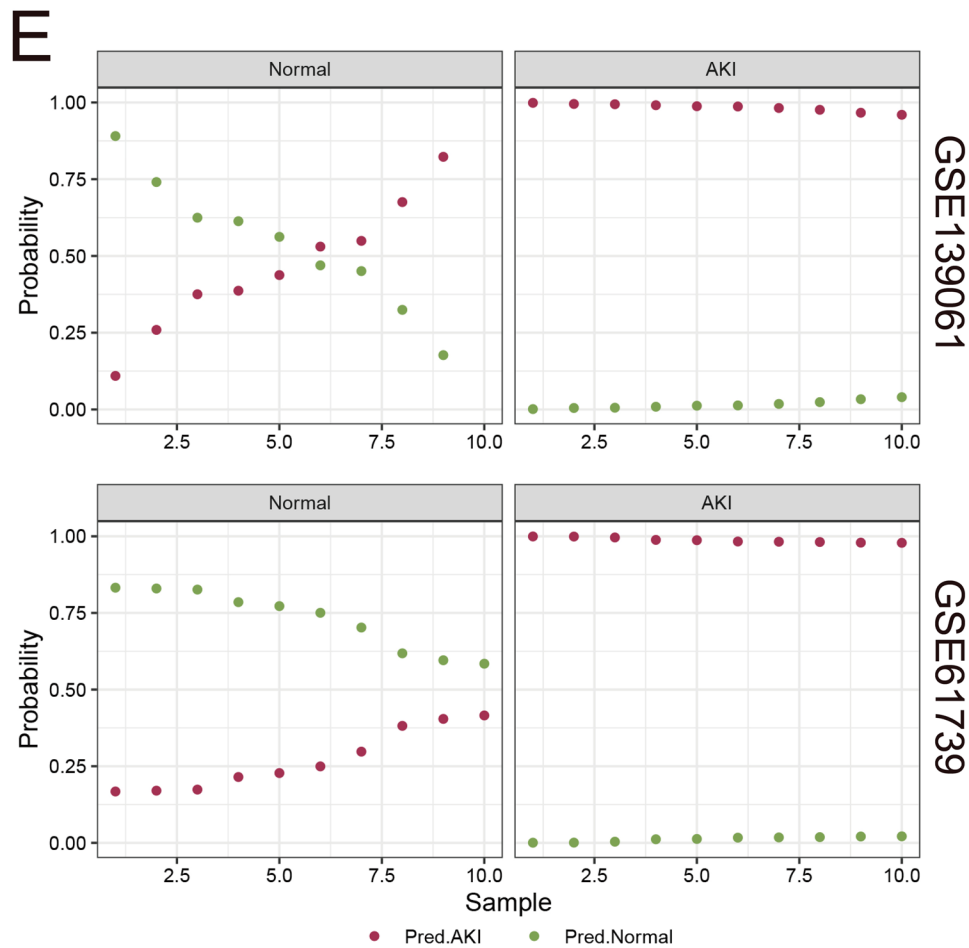
Figure 3. (Continued)

enhanced the proliferative capacity of HK-2 cells (Figure 7(c-d)). Additionally, Transwell assays demonstrated that XRCC3 markedly promoted the migratory ability of HK-2 cells (Figure 7(e)). In addition, flow cytometry revealed that XRCC3 inhibited the number of apoptotic in HK-2 cells (Figure 7(f)). Given that XRCC3 was a mitochondria-associated gene, we examined its impact on mitochondrial function. JC-1 assays showed a significant increase in the percentage of green fluorescence following XRCC3 knockdown, while overexpression of XRCC3 exhibited an increase in the percentage of red fluorescence which indicated that the expression of XRCC3 prominently influenced the mitochondrial membrane potential (Figure 7(g)). The following mitochondrial electron microscopy revealed that XRCC3 knockdown caused mitochondrial shrinkage and a lack of prominent cristae, while XRCC3 overexpression demonstrated clearer mitochondrial architecture (Figure 7(h)). Moreover, mitochondrial immunofluorescence experiments confirmed that the knockdown of XRCC3 led to a decline in mitochondrial structural integrity, whereas overexpression resulted in more intact mitochondrial structures (Figure 7(i)). Therefore, these findings further confirm the role of XRCC3 overexpression in facilitating the proliferation and migratory capacity while inhibiting apoptosis of HK-2 cells. This, in turn, can lead to mitochondrial structural damage

and a reduction in mitochondrial membrane potential, resulting in unhealthy mitochondria and ultimately impairing mitochondrial function, which may exacerbate the progression of AKI.

3.8. The effect of XRCC3 on AKI in vivo

To further elucidate the role of XRCC3 in the progression of AKI, we developed IRI and LPS-induced AKI models in C57BL/6J mice. HE Staining of renal tissues showed severe tubular degeneration, loss of the brush border, and the presence of sloughed debris within the renal tubules across both AKI models, confirming the successful establishment of these models (Figure 8(a)). We subsequently evaluated XRCC3 expression in the AKI models through immunofluorescence analysis, which indicated a significant decrease in XRCC3 levels in AKI mice compared to controls (Figure 8(b)). This result was also corroborated by qRT-PCR analysis (Figure 8(c)). Additionally, we assessed mitochondrial structural changes in both AKI models, which aligned with *in vitro* observations. The electron microscopy demonstrated noticeable mitochondrial shrinkage in the AKI groups, suggesting the presence of unhealthy mitochondria (Figure 8(d)). The following mitochondrial immunofluorescence analysis revealed that mice in
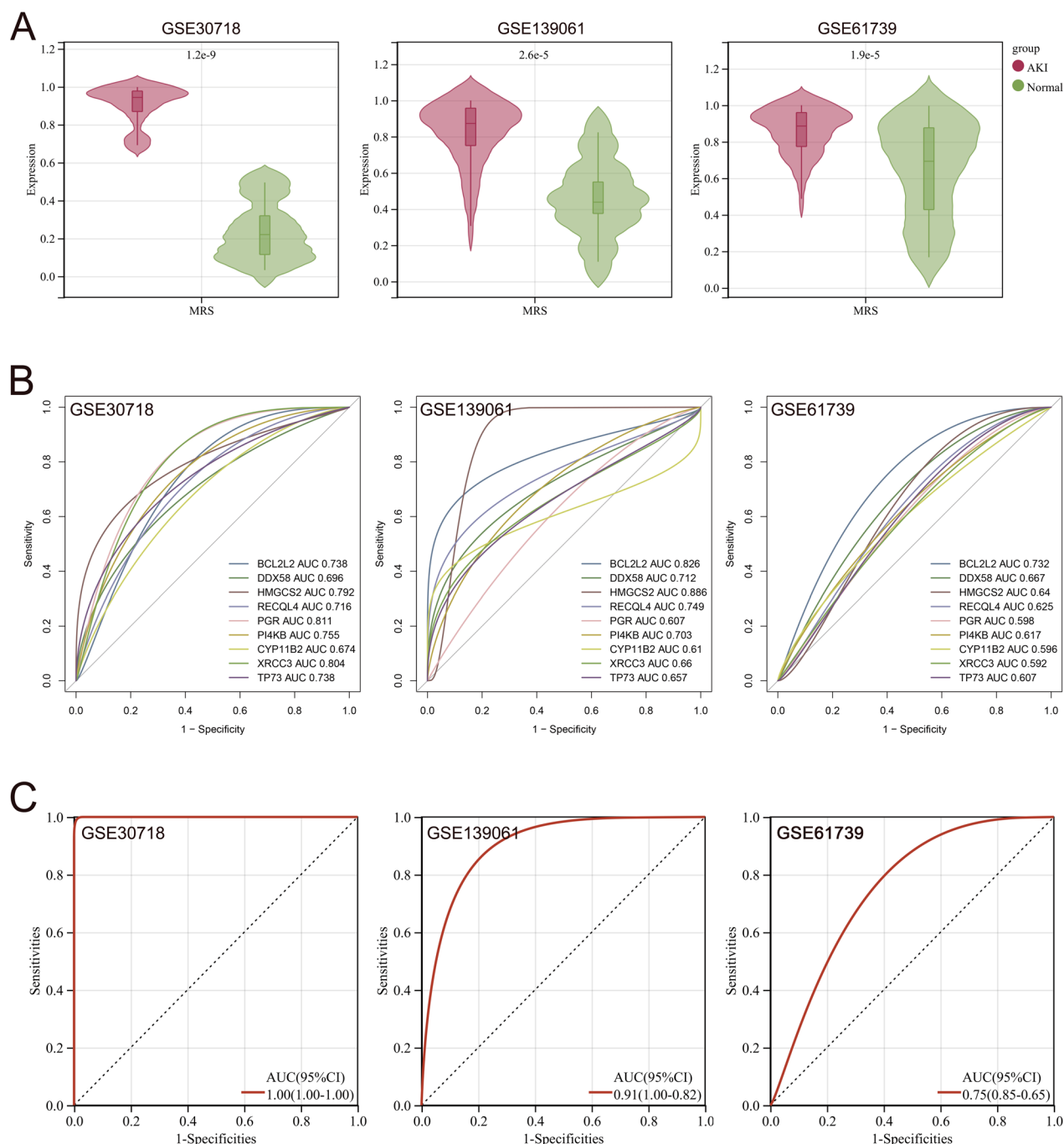
**Figure 4.** Validation of the MRS model for AKI.
(a) Differential expression analysis of MRS between AKI and normal samples in the three datasets, with MRS significantly higher in AKI samples. (b) ROC curve analysis for the nine selected model genes in the three datasets. (c) ROC curve analysis for MRS in the three datasets, demonstrating superior predictive performance compared to individual genes, with AUC values of 1.0 in GSE30718, 0.91 in GSE139061, and 0.75 in GSE61739.

the AKI groups exhibited significantly impaired mitochondrial integrity relative to the normal group (Figure 8(e)).

4. Discussion

AKI is a critical condition marked by a rapid decline in renal function, often resulting from ischemia, nephrotoxins, or sepsis [19]. Mitochondrial dysfunction plays a central role in

AKI pathogenesis, as it disrupts mitochondrial dynamics, impairs energy production, and triggers apoptosis and inflammation [8,20]. These processes significantly contribute to renal injury. Beyond being a consequence of AKI, mitochondrial damage also facilitates the progression to CKD, with persistent mitochondrial dysfunction exacerbating long-term kidney damage [21]. Our findings highlight the importance of mitochondrial-related genes in AKI and
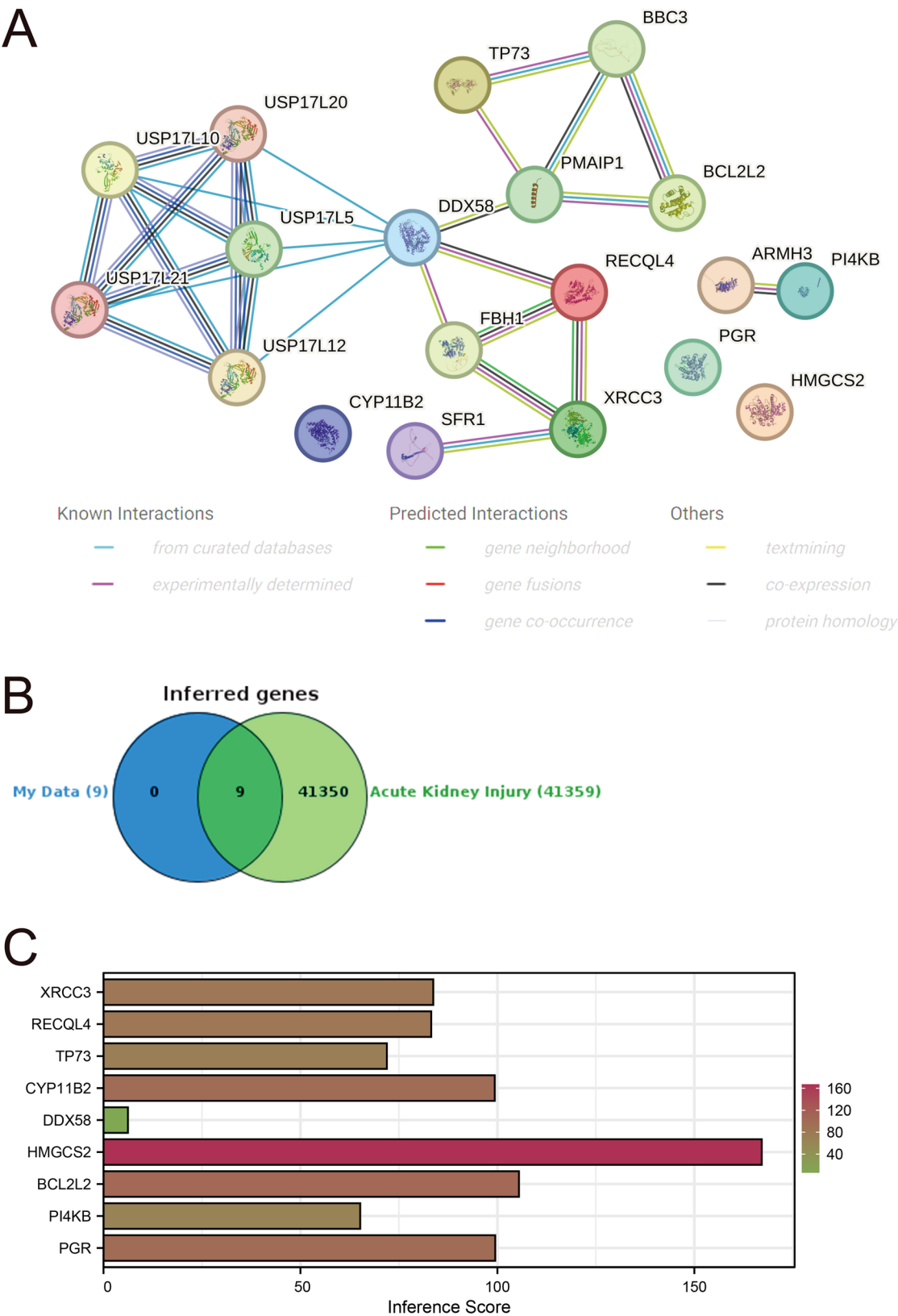
Figure 5. Network and disease mechanism analysis of the nine selected genes for AKI prediction.
(a) PPI network of the nine selected genes constructed using the STRING database. (b) Venn diagram based on CTD database analysis, showing that all nine selected genes are associated with AKI-related genes. (c) Inference scores of the nine selected genes in AKI, with HMGCS2 having the highest score and XRCC3 also showing a significant score, indicating their key roles in AKI pathogenesis.
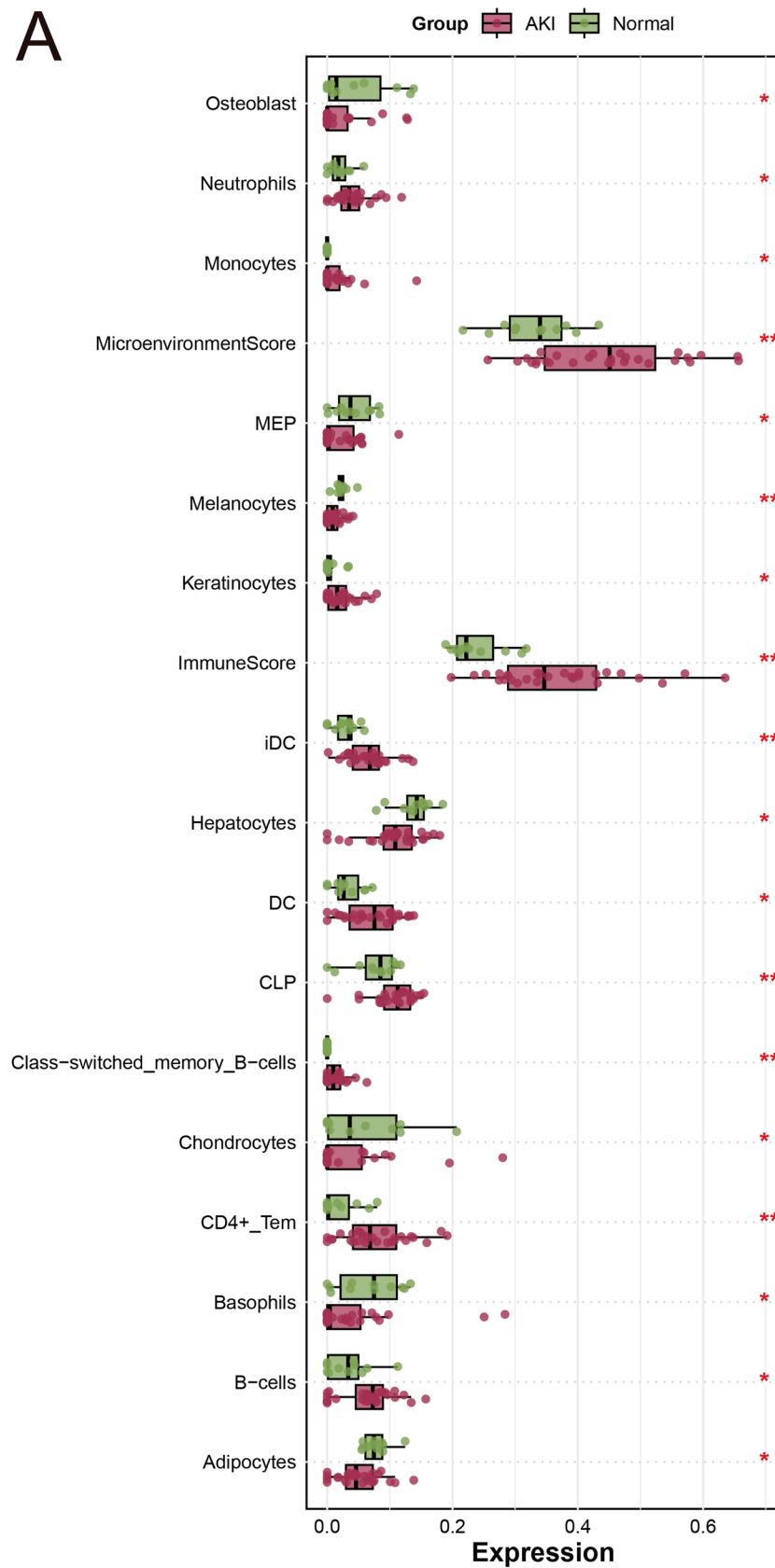
Figure 6. Immune infiltration analysis in AKI and its association with MRS.
(A) Differential expression analysis of immune-related features between AKI and normal samples based on the xCell algorithm, highlighting significant immune alterations in AKI. (B) Comparison of ImmuneScore, StromaScore, and MicroenvironmentScore between high and low MRS patients in AKI, with high MRS patients showing significantly higher ImmuneScores. (C) Correlation analysis between the nine selected model genes and ImmuneScore, revealing strong associations that suggest their involvement in immune modulation in AKI. *$p < 0.05$, **$p < 0.01$, t-test based p-value.
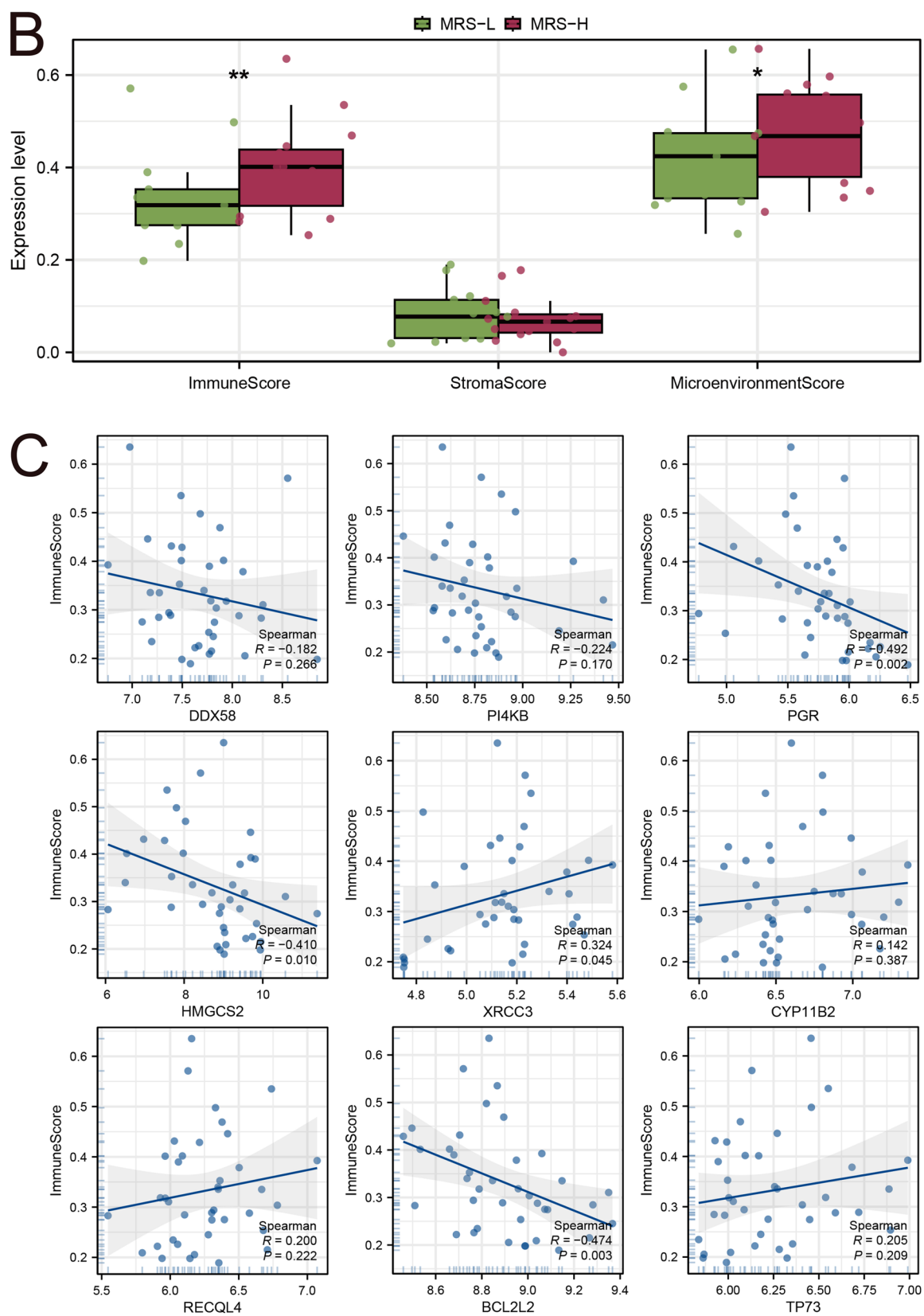
Figure 6. (Continued)
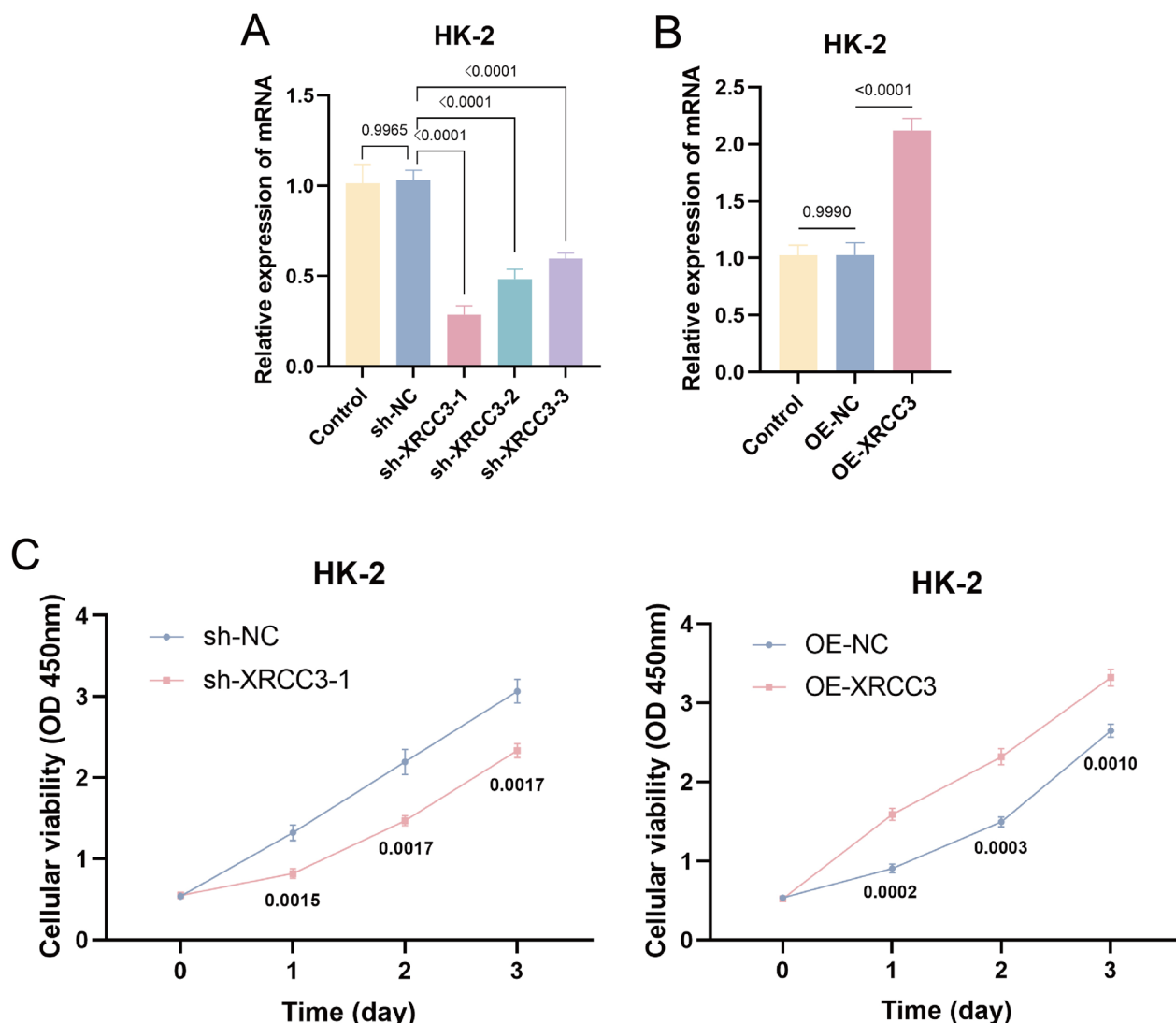
Figure 7. The effect of XRCC3 on HK-2 cell functions.

(a) The results of the qRT-PCR experiments indicated the efficiency of shRNA lentiviral-mediated knockdown of XRCC3 expression, with sh-XRCC3-1 exhibiting the highest knockdown efficacy for following experiments. (b) The results of the qRT-PCR experiments demonstrated the efficiency of lentiviral-mediated overexpression of XRCC3. (c) The results of CCK8 assays showed that silencing the expression of XRCC3 inhibited the proliferation ability while enhancing the expression of XRCC3 facilitated the proliferation ability of HK-2 cells. (d) The EdU assays demonstrated that XRCC3 prominently enhanced the proliferation ability of HK-2 cells (magnification: 200×, bar = 100 μm). (e) Transwell assays indicated that XRCC3 promoted the migration ability of HK-2 cells (magnification: 100×, bar = 120 μm). (f) Apoptosis assays demonstrated that XRCC3 inhibited the number of apoptotic in HK-2 cells. (g) JC-1 staining assays indicated that XRCC3 influenced the mitochondrial membrane potential as the green fluorescence presented the low electric potential and the red fluorescence presented the high electric potential. (h) Electron microscopy results of mitochondrial structure (magnification: 20,000×, bar = 500 nm). (i) Mitochondrial immunofluorescence results demonstrated that XRCC3 could maintain the integrity of the mitochondrial structure (magnification: 400×, bar = 20 μm). Each experiment was performed independently at least three times to ensure reproducibility.

suggest their potential as biomarkers for early diagnosis and prognosis.

With the advancement of bioinformatics, integrating large-scale multi-omics data has become increasingly feasible, allowing for more nuanced insights into disease mechanisms. This approach is not only valuable in cancer research, where molecular signatures and immune modulation have been extensively studied, but it also shows great promise in non-cancerous conditions, such as AKI [22–24]. In this study, we identified a set of mitochondrial-related genes that are consistently dysregulated in AKI, providing novel insights into the role of mitochondrial dysfunction in the

pathogenesis of kidney injury. Using publicly available datasets (GSE30718, GSE61739, and GSE139061), we developed a predictive model based on nine mitochondrial-related genes that demonstrated high sensitivity and specificity in distinguishing AKI from normal samples. Furthermore, our analysis revealed a significant association between mitochondrial dysfunction and immune cell infiltration in AKI, suggesting an intricate relationship between metabolic disturbances and inflammatory responses in the kidney.

Functional enrichment analysis of DEGs provided valuable insights into the molecular mechanisms underlying AKI. These findings of upregulated genes suggest that AKI induces
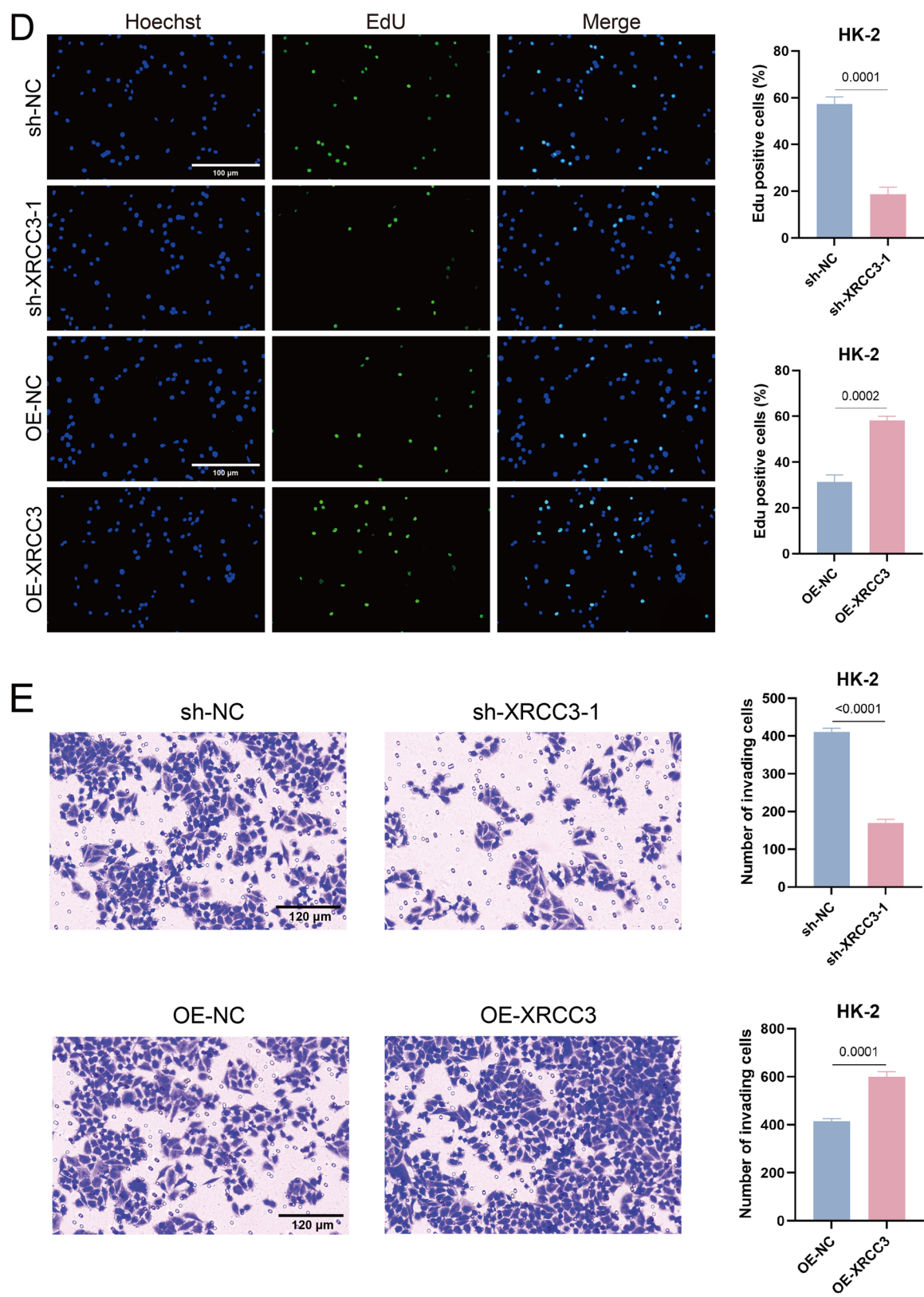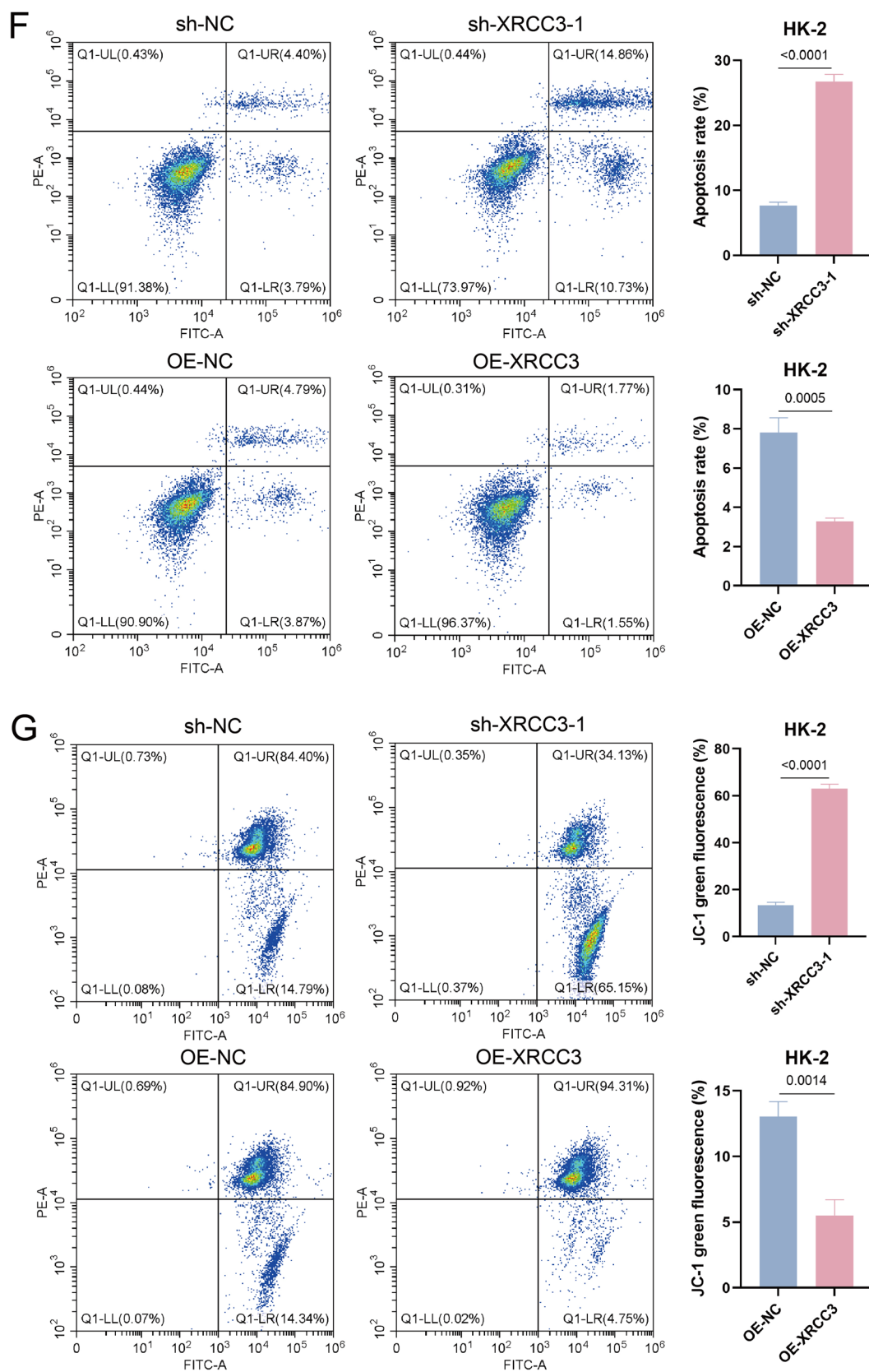
Figure 7. (Continued)

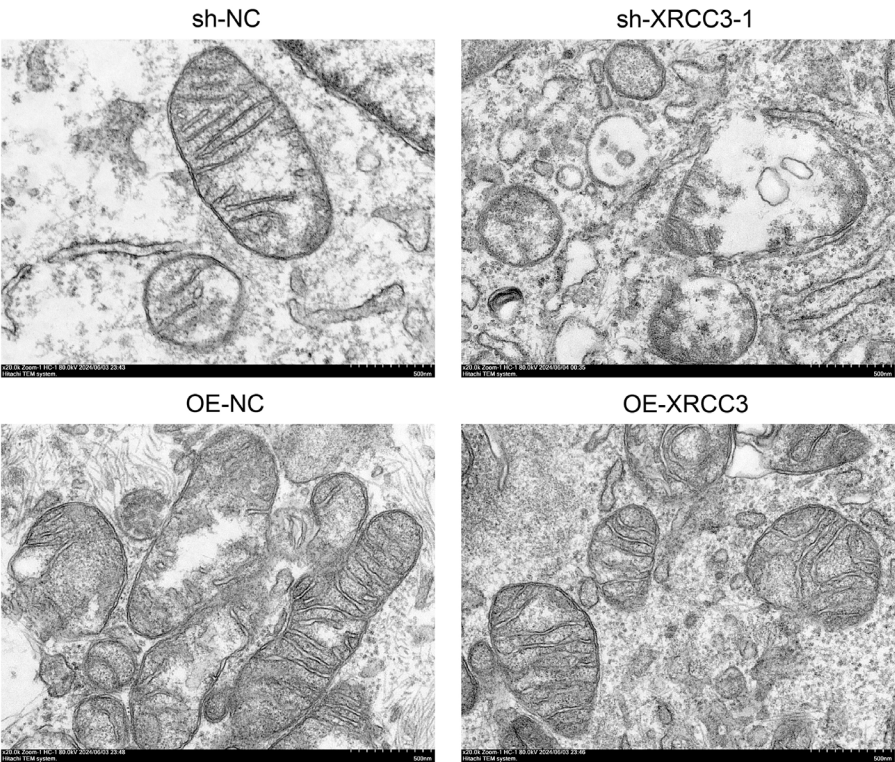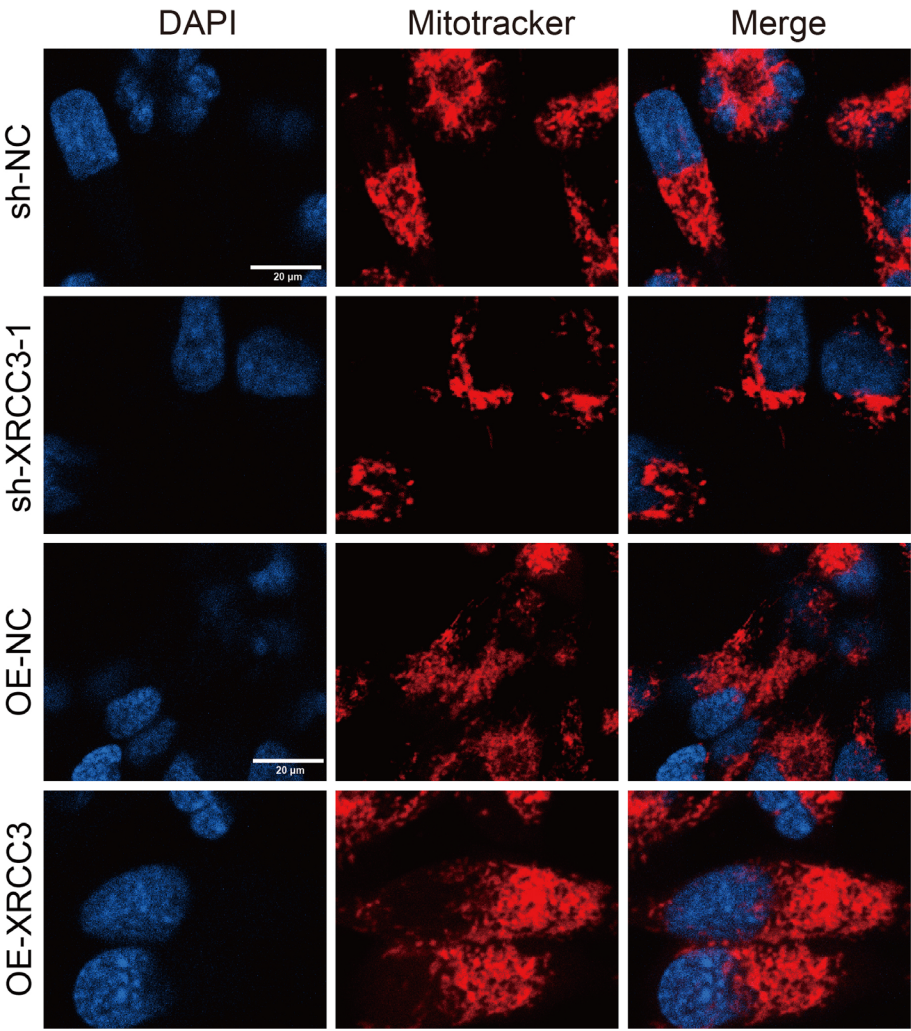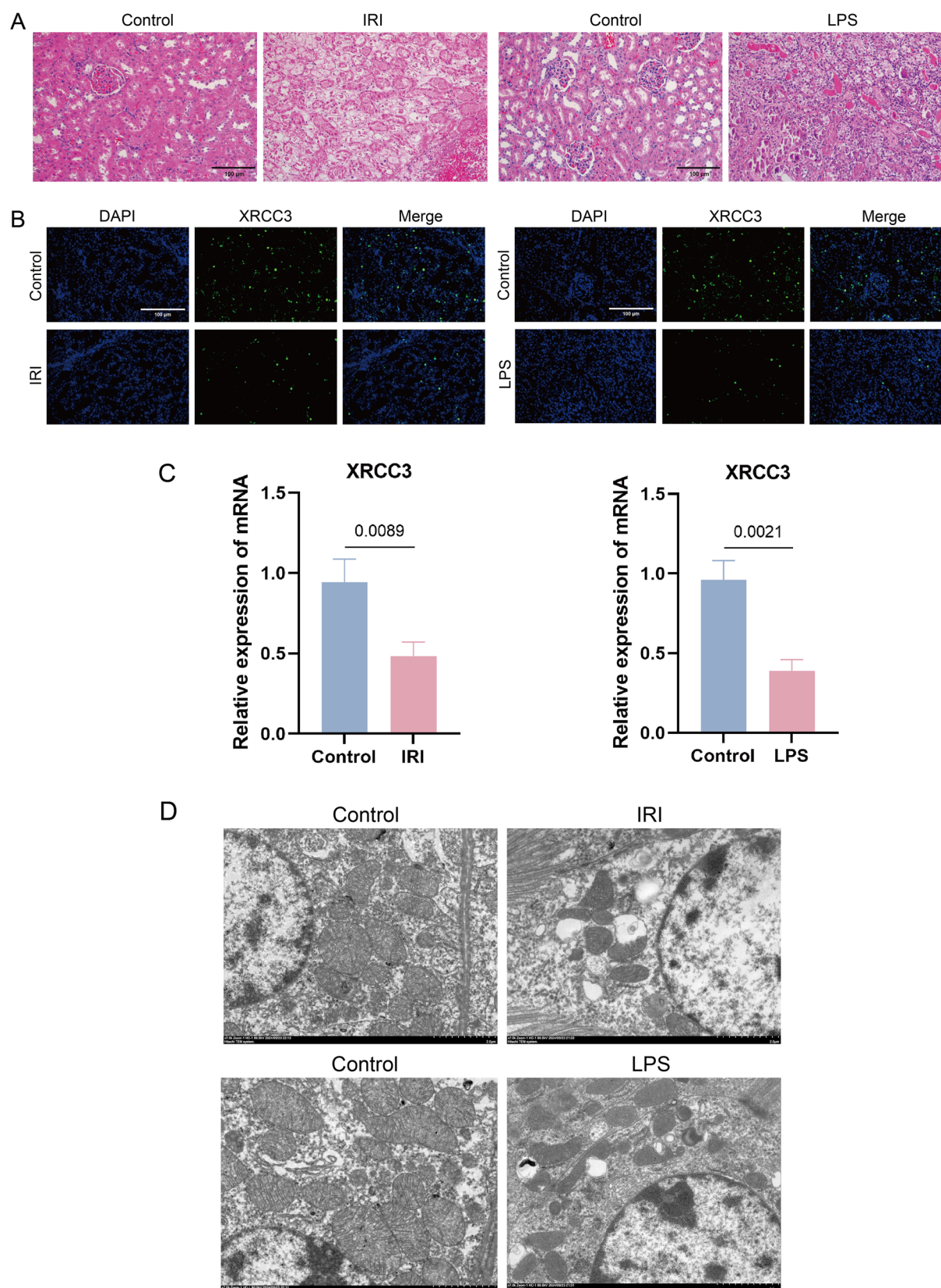**Figure 7.** (Continued)

Figure 7. (Continued)

Figure 8. The effect of XRCC3 on AKI *in vivo*.
(a) Representative HE staining images of the IRI and LPS-induced AKI models, which were utilized for assessing the success of the model construction (magnification: 200×, bar = 100 μm). (b) The immunofluorescence experiment was conducted to examine the expression levels of XRCC3 in the AKI model compared to the control group (magnification: 200×, bar = 100 μm). (c) The results of the qRT-PCR demonstrated the expression levels of XRCC3 in both the AKI model and the control group. (d) The results of mitochondrial morphological changes observed under electron microscopy in both the AKI group and the control group (magnification: 7000×, bar = 2 μm). (e) The mitochondrial immunofluorescence assays in the AKI and the control group illustrated the alterations in mitochondrial structural integrity (magnification: 100×, bar = 100 μm). Each experiment was performed independently at least three times to ensure reproducibility.
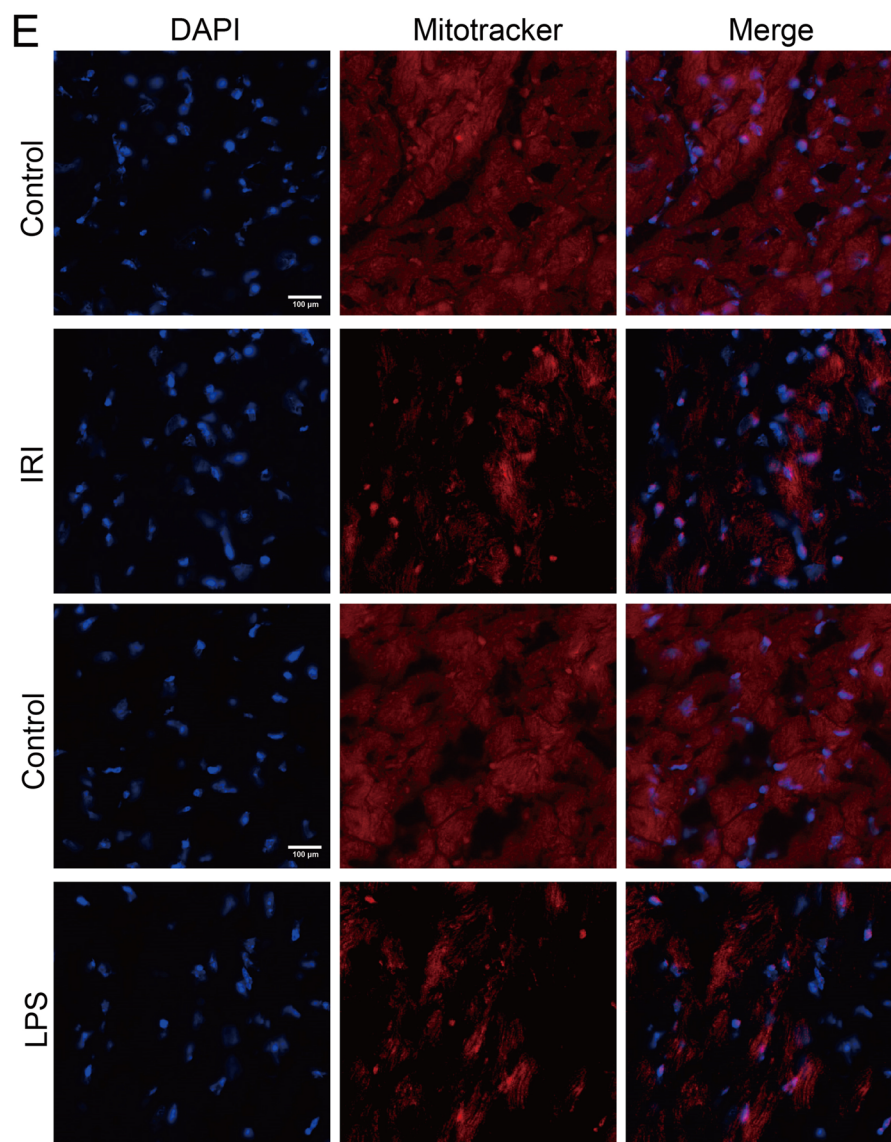
Figure 8. (Continued)

significant tissue remodeling and cellular adaptations [25–27]. Conversely, downregulated genes were strongly associated with mitochondrial functions, including the mitochondrial matrix, inner membrane, and amino acid metabolism, indicating mitochondrial dysfunction as a key feature of AKI [28–29]. KEGG pathway analysis further revealed that upregulated genes were linked to immune-related pathways like Salmonella infection and neuroactive ligand-receptor interactions, while downregulated genes were enriched in metabolic pathways such as Tryptophan metabolism and Nonalcoholic fatty liver disease [30–31]. Collectively, these results highlight the central role of mitochondrial dysfunction, immune dysregulation, and metabolic disturbances in AKI pathogenesis.

The MRS, which combines the expression levels of nine selected mitochondrial genes, exhibits a markedly enhanced predictive performance in comparison to individual gene assessments. This observation supports the hypothesis that AKI is a multifaceted condition, wherein various molecular pathways, including mitochondrial dysfunction, contribute to the disease's progression. Mitochondrial damage can induce cellular stress and elicit the release of pro-inflammatory mediators, which in turn activate the immune response and facilitate the recruitment of immune cells into renal tissue. In addition, This observation is also in line with studies indicating that mitochondrial dysfunction can influence immune responses by activating inflammasomes and promoting inflammatory cascades, further exacerbating kidney injury [32–33]. Several studies have reported that XRCC2 is involved in various pathways regulating the occurrence and progression of cancers, such as liver cancer, colorectal cancer, and lung cancer, and have identified multiple therapeutic targets centered on XRCC2 as a key molecule [34–37]. However, the potential molecular mechanisms linking XRCC2 to AKI remain to be elucidated, and our findings

provide new insights and perspectives in this regard. Additionally, research has shown that LONP1 can target HMGCS2 to mitigate CKD, with findings indicating that aging and normal glomeruli are associated with decreased expression of CYP11B2 and increased expression in clusters producing aldosterone. Excessive aldosterone has been linked to accelerated progression of CKD [38–39]. Therefore, the MRS we have identified plays a crucial regulatory role in kidney diseases, and further exploration of the molecular mechanisms of MRS in AKI may offer novel therapeutic targets.

However, several limitations should be considered. First, our study relies on bioinformatics analysis of publicly available datasets, which may introduce biases due to differences in sample collection, processing, and platform variations. The generalizability of the identified biomarkers and predictive model should be validated in independent clinical cohorts. Furthermore, while we focused on the dysregulation of mitochondrial genes, functional validation of these genes and their specific roles in AKI pathogenesis is necessary to establish causal relationships, although MRS is significantly correlated with immune infiltration, it does not further demonstrate a correlation between immune cell infiltration and the severity of AKI and the specific mechanism of MRS regulates immune infiltration of AKI remains to elucidate. In addition, the study does not address potential therapeutic interventions targeting mitochondrial dysfunction, which warrants investigation in preclinical models.

In conclusion, our findings underscore the central role of mitochondrial dysfunction in AKI and provide a foundation for the development of mitochondrial-based biomarkers for early diagnosis and prognosis. The predictive model we developed holds promise for clinical application, and further exploration of mitochondrial-targeted therapies could significantly improve outcomes for patients suffering from AKI.

Acknowledgments

Authors contributions

CRediT: **Xiaoping Xia**: Formal analysis, Funding acquisition, Software, Validation, Writing – original draft, Writing – review & editing; **Renyang Liu**: Data curation, Investigation, Writing – review & editing; **Xiaohui Jiang**: Conceptualization, Methodology, Project administration, Resources, Supervision, Writing – review & editing.

Ethics approval and consent to participate

All experiments were approved by the Institutional Animal Care and Use Committee of the Hubei Provincial Center for Disease Control and Prevention (License Number: 202410107). The publicly available datasets do not require additional ethical approval.

Disclosure statement

Funding

ORCID

Xiaohui Jiang http://orcid.org/0009-0009-0128-8142

Data availability statement

All data generated or analyzed during this study are included in this published article and its supplementary information files.

References

[1] Kellum JA, Romagnani P, Ashuntantang G, et al. Acute kidney injury. Nat Rev Dis Primers. 2021;7(1):52. doi: 10.1038/s41572-021-00284-z.

[2] Pickkers P, Darmon M, Hoste E, et al. Acute kidney injury in the critically ill: an updated review on pathophysiology and management. Intensive Care Med. 2021;47(8):835–850. doi: 10.1007/s00134-021-06454-7.

[3] Ronco C, Bellomo R, Kellum JA. Acute kidney injury. Lancet. 2019;394(10212):1949–1964. doi: 10.1016/S0140-6736(19)32563-2.

[4] Hoste EAJ, Kellum JA, Selby NM, et al. Global epidemiology and outcomes of acute kidney injury. Nat Rev Nephrol. 2018;14(10):607–625. doi: 10.1038/s41581-018-0052-0.

[5] Chawla LS, Bellomo R, Bihorac A, et al. Acute kidney disease and renal recovery: consensus report of the Acute Disease Quality Initiative (ADQI) 16 Workgroup. Nat Rev Nephrol. 2017;13(4):241–257. doi: 10.1038/nrneph.2017.2.

[6] Nunnari J, Suomalainen A. Mitochondria: in sickness and in health. Cell. 2012;148(6):1145–1159. doi: 10.1016/j.cell.2012.02.035.

[7] Emma F, Montini G, Parikh SM, et al. Mitochondrial dysfunction in inherited renal disease and acute kidney injury. Nat Rev Nephrol. 2016;12(5):267–280. doi: 10.1038/nrneph.2015.214.

[8] Tang C, Cai J, Yin X-M, et al. Mitochondrial quality control in kidney injury and repair. Nat Rev Nephrol. 2021;17(5):299–318. doi: 10.1038/s41581-020-00369-0.

[9] Galvan DL, Green NH, Danesh FR. The hallmarks of mitochondrial dysfunction in chronic kidney disease. Kidney Int. 2017;92(5):1051–1057. doi: 10.1016/j.kint.2017.05.034.

[10] Szeto HH. Pharmacologic approaches to improve mitochondrial function in AKI and CKD. J Am Soc Nephrol. 2017;28(10):2856–2865. doi: 10.1681/ASN.2017030247.

[11] Cleveland KH, Schnellmann RG. Pharmacological targeting of mitochondria in diabetic kidney disease. Pharmacol Rev. 2023;75(2):250–262. doi: 10.1124/pharmrev.122.000560.

[12] Wang H, Li Y, Liu X, et al. Identification and validation of ferroptosis-related gene SLC2A1 as a novel prognostic biomarker in AKI. Aging (Albany NY). 2024;16(6):5634–5650. doi: 10.18632/aging.205669.

[13] Li J, Zhu M, Yan L. Predictive models of sepsis-associated acute kidney injury based on machine learning: a scoping review. Ren Fail. 2024;46(2):2380748. doi: 10.1080/0886022X.2024.2380748.

[14] Yang S, Guo J, Xiong Y, et al. Unraveling the genetic and molecular landscape of sepsis and acute kidney injury: a comprehensive GWAS and machine learning approach. Int Immunopharmacol. 2024;137:112420. doi: 10.1016/j.intimp.2024.112420.

[15] Zhang X, Wu H, Niu J, et al. A novel mitochondria-related gene signature in esophageal carcinoma: prognostic, immune, and therapeutic features. Funct Integr Genomics. 2023;23(2):109. doi: 10.1007/s10142-023-01030-2.

[16] Szklarczyk D, Kirsch R, Koutrouli M, et al. The STRING database in 2023: protein-protein association networks and functional enrichment analyses for any sequenced genome of interest. Nucleic Acids Res. 2023;51(D1):D638–d646. doi: 10.1093/nar/gkac1000.

[17] Davis AP, Wiegers TC, Johnson RJ, et al. Comparative toxicogenomics database (CTD): update 2023. Nucleic Acids Res. 2023;51(D1):D1257–d1262. doi: 10.1093/nar/gkac833.

[18] Aran D, Hu Z, Butte AJ. xCell: digitally portraying the tissue cellular heterogeneity landscape. Genome Biol. 2017;18(1):220. doi: 10.1186/s13059-017-1349-1.

[19] Juncos LA, Wieruszewski PM, Kashani K. Pathophysiology of acute kidney injury in critical illness: a narrative review. Compr Physiol. 2022;12(4):3767–3780. doi: 10.1002/j.2040-4603.2022.tb00231.x.

[20] Lin HY-H, Chen Y, Chen Y-H, et al. Tubular mitochondrial AKT1 is activated during ischemia reperfusion injury and has a critical role in predisposition to chronic kidney disease. Kidney Int. 2021;99(4):870–884. doi: 10.1016/j.kint.2020.10.038.

[21] Liu X, Zhang Y, Wang Y, et al. Tubular MYDGF slows progression of chronic kidney disease by maintaining mitochondrial homeostasis. Adv Sci (Weinh). 2025;12(3):e2409756. doi: 10.1002/advs.202409756.

[22] Rudman-Melnick V, Adam M, Potter A, et al. Single-cell profiling of AKI in a murine model reveals novel transcriptional signatures, profibrotic phenotype, and epithelial-to-stromal crosstalk. J Am Soc Nephrol. 2020;31(12):2793–2814. doi: 10.1681/ASN.2020010052.

[23] Wang Y, Shao W, Feng Y, et al. Prognostic value and potential biological functions of ferroptosis-related gene signature in bladder cancer. Oncol Lett. 2022;24(3):301. doi: 10.3892/ol.2022.13421.

[24] Zhang D, Zhao K, Han T, et al. Bisphenol A promote the cell proliferation and invasion ability of prostate cancer cells via regulating the androgen receptor. Ecotoxicol Environ Saf. 2024;269:115818. doi: 10.1016/j.ecoenv.2023.115818.

[25] Nawaz M, Shah N, Zanetti BR, et al. Extracellular vesicles and matrix remodeling enzymes: the emerging roles in extracellular matrix remodeling, progression of diseases and tissue repair. Cells. 2018;7(10):167. doi: 10.3390/cells7100167.

[26] Wang H, Gao M, Li J, et al. MMP-9-positive neutrophils are essential for establishing profibrotic microenvironment in the obstructed kidney of UUO mice. Acta Physiol (Oxf). 2019;227(2):e13317. doi: 10.1111/apha.13317.

[27] Wijerathne CUB, Au-Yeung KKW, Siow YL, et al. 5-Methyltetrahydrofolate attenuates oxidative stress and improves kidney function in acute kidney injury through activation of Nrf2 and antioxidant defense. Antioxidants (Basel). 2022;11(6):1046. doi: 10.3390/antiox11061046.

[28] Oe Y, Vallon V. CRRT 2023 meeting: targeting amino acid transport to improve acute kidney injury outcome. Nephron. 2023;147(12):774–777. doi: 10.1159/000531918.

[29] Tang W, Wei Q. The metabolic pathway regulation in kidney injury and repair. Front Physiol. 2023;14:1344271. doi: 10.3389/fphys.2023.1344271.

[30] Gaut JP, Liapis H. Acute kidney injury pathology and pathophysiology: a retrospective review. Clin Kidney J. 2021;14(2):526–536. doi: 10.1093/ckj/sfaa142.

[31] Abbasi HQ. Comments on: nonalcoholic fatty liver disease predicts acute kidney injury readmission in heart failure hospitalizations: a nationwide analysis. Curr Probl Cardiol. 2023;48(11):101943. doi: 10.1016/j.cpcardiol.2023.101943.

[32] Li P, Zhou M, Wang J, et al. Important role of mitochondrial dysfunction in immune triggering and inflammatory response in rheumatoid arthritis. J Inflamm Res. 2024;17:11631–11657. doi: 10.2147/JIR.S499473.

[33] Mishra Y, Kumar A, Kaundal RK. Mitochondrial dysfunction is a crucial immune checkpoint for neuroinflammation and neurodegeneration: mtDAMPs in focus. Mol Neurobiol. 2024. Online ahead of print. doi: 10.1007/s12035-024-04412-0.

[34] Greenhough LA, Liang C-C, Belan O, et al. Structure and function of the RAD51B-RAD51C-RAD51D-XRCC2 tumour suppressor. Nature. 2023;619(7970):650–657. doi: 10.1038/s41586-023-06179-1.

[35] Zhao Z, He K, Zhang Y, et al. XRCC2 repairs mitochondrial DNA damage and fuels malignant behavior in hepatocellular carcinoma. Cancer Lett. 2021;512:1–14. doi: 10.1016/j.canlet.2021.04.026.

[36] Gong H, Zhang P, Liu Q, et al. XRCC2 driven homologous recombination subtypes and therapeutic targeting in lung adenocarcinoma metastasis. NPJ Precis Oncol. 2024;8(1):169. doi: 10.1038/s41698-024-00658-y.

[37] Qin C, Ji Z, Zhai E, et al. PARP inhibitor olaparib enhances the efficacy of radiotherapy on XRCC2-deficient colorectal cancer cells. Cell Death Dis. 2022;13(5):505. doi: 10.1038/s41419-022-04967-7.

[38] Tuttle KR, Hauske SJ, Canziani ME, et al. Efficacy and safety of aldosterone synthase inhibition with and without empagliflozin for chronic kidney disease: a randomised, controlled, phase 2 trial. Lancet. 2024;403(10424):379–390. doi: 10.1016/S0140-6736(23)02408-X.

[39] Nanba K, Vaidya A, Williams GH, et al. Age-related autonomous aldosteronism. Circulation. 2017;136(4):347–355. doi: 10.1161/CIRCULATIONAHA.117.028201.